Analysis of structural dynamics and damping performance of a beam-tendon system undergoing large shape changes

S. Jayatilake, B. Woods, M. Lowenberg, B. Titurus
University of Bristol, Department of Aerospace Engineering,
Bristol, UK
e-mail: **sj17967@bristol.ac.uk**

Abstract

This paper investigates modal characteristics presented by a slender beam supporting an axially elastic tendon guided across a series of points placed eccentrically along the beam span. The nonlinear structural model is developed based on the Rayleigh-Ritz method, incorporating an energy-based approach combined with a shape function discretisation. The system is studied numerically, focusing on the modal characteristics induced by the pre-stress carried by the tendon network, along with its axially viscoelastic properties. Initial experimental comparison is presented substantiating the numerically observed frequency trends induced by the applied tension. The mode-specific effects of the applied tension and stiffness and the trends observed on the natural frequencies are demonstrated with modal information extracted about the nonlinear static equilibria. The effect of axial damping is also considered to demonstrate its influence on vibration modes in the tendon-loaded beam structure.

1 Introduction

With the ever-increasing significance in mass transportation, the development of aircraft with enhanced efficiency continues to influence the aerospace community and industry globally. Whilst this aspiration is addressed across multiple disciplines ranging from propulsion to efficient structural designs, a key enabler is recognised in the form aircraft with novel wing architectures such as high aspect ratio wings (HARWs), owing to their promise of reduced induced drag.

However, HARW designs are often susceptible to a range of challenges. With the exception practical aspects such as span-limitation at airports, these challenges are dictated by the aeroelastic instabilities 0. These are largely a result of the inevitable structural slenderness of these designs that is a result of the need to ensure that the aerodynamic benefit from the design is not negated by added structural weight. HARW wing designs exhibit highly nonlinear characteristics, including ones of structural geometric nature due to large deformations. Such nonlinearities can highly alter the dynamic/modal properties of the system at increasing levels of deformation and introduce new forms of bend-twist coupling which encourages aeroelastic instabilities 0. Significant research effort surrounding the development of passive means of delaying such instabilities and the suppression of post-instability activity can be identified. With the exception of aeroelastic tailoring (e.g., using tow-steered composites), this often consists of the introduction of discrete devices such as nonlinear energy sinks (NES) 0 and distributed damping systems such as viscoelastic layers or piezoelectric patches 0, 0. Such devices often have their own limitations, such as the extent of the required mass and stiffness, integrability within constrained spaces and operating conditions due to limited frequency or thermal characteristics.

Among numerous research developments of systems influencing structural dynamics and vibration control, efforts surrounding the use of tendons (cables) continue to attract significant interest, particularly in civil engineering applications 0, 0. These concepts often targeted the development of the seismic protection measures in various forms of built infrastructure, for example through fitting of the embedded cable-pulley systems allowing the induced axial activity of the cable to be integrated with the discrete energy dissipation

devices. Another recent work aimed towards rotorcraft applications also investigates the efficient use of the blade-embedded tendons with intermittent guides 0. There, the tendon is modelled as a cable under constant tension undergoing transverse displacements. Efforts like this mainly focus on the natural frequency tuning effect of the applied axial loading for resonance avoidance. Alternatively, more recent developments introduced soft guiding elements with integrated energy absorbing compliant elements which exploit the highly coupled blade-tendon modal activity 0. It was demonstrated that this approach can be highly effective at introducing mode targeted damping and suppressing resonant behaviour. To complement this research, the present work intends to expand the understanding of the impact of the induced axial tendon activity, akin to the abovementioned civil engineering applications, in the context of slender structures that can experience moderate to large transversal deformations.

The aim here is to investigate an embedded network formed by a guided axially soft tendon. This work combines the views used for seismic control and the use of the embedded tendons to introduce a novel dynamic tuning strategy. The system studied herewith builds up from 0, encapsulating a single axially elastic tendon, guided across a series of points placed eccentrically across the beam structure. The novelty of this work stems from the modelling of the axial tendon activity and the investigation of the influence of the applied pre-tension, axial stiffness and damping on the overall dynamic characteristics. The investigated system holds the potential of being a generic and adaptively controllable platform that allows for a synthesis between tendons and other more localized energy dissipation systems such as NES. This paper deals with the initial modelling and analysis work, combined with initial comparisons against the benchtop experiment. The analysis of the system is developed with a focus towards HARW applications, with an appreciation of geometric nonlinearities and its influences on the modal properties. In particular, the study of modal characteristics carried out herewith is comparable to the methods utilised in 0, where the modal properties were assessed about the topologically accurate linearisations obtained from nonlinear static equilibria.

Accordingly, the paper is structured as follows: Section 2 provides an overview of the nonlinear model, particularly the context behind the modelling of the tendon system. Initial experimental comparisons are demonstrated next in section 3, aiming to evaluate the developed model within the real experimental context. Following this, section 4 uses the model to illustrate the dynamic characteristics and their changes on a beam structure comparable to a HARW.

2 Model description

2.1 Structural model and geometrical descriptions

The structural model developed for the purpose of the present analysis is largely based on 0, with a particular focus on the simplicity of capturing geometrical aspects enabling the integration of other elements gradually. The model is developed utilising the Rayleigh-Ritz approach, with the polynomial shape functions discretising the out-of-plane displacements w and in-plane displacements v of the elastic axis and the torsion θ defined within the plane of a local cross-section (see Figure 1). Accordingly, these transversal and rotational displacements, which appear explicitly in the final equations of motion, are discretised using a series of shape functions in the form:

$$w(s,t) = \mathbf{W}(s)^{\mathrm{T}}\mathbf{q}_w, \qquad \theta(s,t) = \mathbf{\Theta}(s)^{\mathrm{T}}\mathbf{q}_\theta, \qquad v(s,t) = \mathbf{V}(s)^{\mathrm{T}}\mathbf{q}_v \tag{1}$$

where $\mathbf{W}(s) \in \mathbb{R}^{N_w}$, $\mathbf{\Theta}(s) \in \mathbb{R}^{N_\theta}$,$\mathbf{V}(s) \in \mathbb{R}^{N_v}$ are the shape functions vectors (arrays) described as a function of the arc length along the elastic axis and $\mathbf{q}_w, \mathbf{q}_\theta, \mathbf{q}_v$ are the time varying generalised coordinates. Later, $\mathbf{q}^{\mathrm{T}} = \begin{bmatrix} \mathbf{q}_w^{\mathrm{T}} & \mathbf{q}_\theta^{\mathrm{T}} & \mathbf{q}_v^{\mathrm{T}} \end{bmatrix}$ is used as an overall generalised vector of the augmented wing.

The kinematic model description comprises of two essential sets of axes: Frame $O(\mathbf{i}, \mathbf{j}, \mathbf{k})$ is fixed at the root and frame $A(\mathbf{e}_\mathbf{x}, \mathbf{e}_\mathbf{y}, \mathbf{e}_\mathbf{z})$ remains local to a cross-section of interest (with $\mathbf{e}_\mathbf{x}$ being the cross-sectional

normal) and the vector $\mathbf{e}_y$ is placed at an angle θ from the plane $O(x, y)$, measured along the plane of the local cross-section.

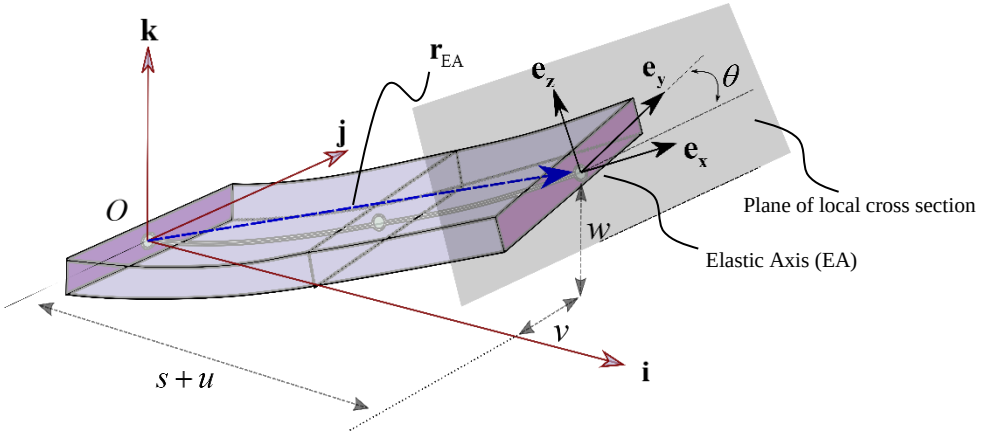

Figure 1: Geometrical definitions of displacements, angular components and frames

A beam possesses a straight elastic axis which is initially aligned with the *x* axis. From this undeformed position, the local displacements of each point along the elastic axis are given by, $\begin{bmatrix} u(s,t) & v(s,t) & w(s,t) \end{bmatrix}^{\mathrm{T}}$, where s,t define the arc length along the elastic axis from the origin O and the time instance, respectively. Alternatively, a point at an arc-length wise position s along the elastic axis, initially situated at $\begin{bmatrix} s & 0 & 0 \end{bmatrix}^{\mathrm{T}}$, displaces to the point $\mathbf{r}_{\mathrm{EA}} = \begin{bmatrix} s+u(s,t) & v(s,t) & w(s,t) \end{bmatrix}^{\mathrm{T}}$. Note that, in the development, the horizontal displacement is implied implicitly in terms of the transversal deformations through the enforcement of the inextensibility constraint given by $(1+u')^2 + w'^2 + v'^2 = 1$.

The vectors defining the axes of the frame are derived implicitly as functions of the abovementioned transversal and rotational deformations through the geometrical arguments. Ultimately, these axes are expressed in terms of the generalised coordinates $\mathbf{q}$ defined previously (for instance, $\mathbf{e}_{\mathbf{x}}(\mathbf{q}) = \mathbf{r}'_{\mathrm{EA}}$). With these vectors defined, the instantaneous position vector of a generic point on a cross section of the structure initially at $\begin{bmatrix} x & n_y & n_z \end{bmatrix}^{\mathrm{T}}$ can be described by:

$$\mathbf{r} = \mathbf{r}_{\mathrm{EA}} + n_y \mathbf{e}_{\mathbf{y}} + n_z \mathbf{e}_{\mathbf{z}} \tag{2}$$

where (n_y, n_z) defines an initial position within a given cross sectional face.

The final nonlinear equations of motion are developed based on the Lagrange equation given by:

$$\frac{d}{dt}\left(\frac{\partial \mathrm{L}}{\partial \dot{q}_i}\right) = \frac{\partial \mathrm{L}}{\partial q_i} + Q_i, \qquad i \in \{1 \quad \dots \quad N_w + N_v + N_\theta\} \tag{3}$$

where the Lagrangian is constructed in the form $\mathrm{L} = \mathrm{T} - \mathrm{U}$ of which T and U are the kinetic and the strain energies of the beam derived from the equivalent nonlinear energy expressions obtained from 0. The influence of the external forces on the beam is included after considering infinitesimal work arguments, where $\mathbf{Q} = \begin{bmatrix} Q_1 & \dots & Q_{N_w+N_v+N_\theta} \end{bmatrix}^{\mathrm{T}}$ is a vector of the generalised forces such that $\delta\mathbf{q}^{\mathrm{T}}\mathbf{Q}$ is equivalent to the work imparted on the system under infinitesimal displacements.

2.2 Tendon model

The augmentation discussed herewith comprises of a single axially elastic tendon passed through a series of the guiding points along the length of the beam. The tendon under pre-tension is assumed to be massless, eliminating the need to account for additional transversal degrees of freedom of the tendon: accordingly, the tendon's influence is here simply modelled as a function of the cumulative axial extension between the guiding points, with the axial forces directed along the points joining the adjacent guides as detailed below. In addition to this, the effect of friction originating from the guides is not modelled, while the tension is assumed to be time varying with the constant value across all tendon segments.

A series of tendon guides, $j=1,\ldots,J$ is considered where the guide at $j=1$ is at $s=s_1=0$ such that due to the cantilever boundary condition of the beam, this point is naturally fixed/anchored. The lengthwise position and the offsets along the $\mathbf{e}_\mathbf{y}$ and $\mathbf{e}_\mathbf{z}$ axes of the *j*th guide is given by s_j, n_{y_j} and n_{z_j}, respectively, as illustrated in Figure 2, with its instantaneous position vector being $\mathbf{r}_j$, where from (2),

$$\mathbf{r}_j = \mathbf{r}_{\mathrm{EA}}(s_j) + n_{y_j}\mathbf{e}_\mathbf{y}(s_j) + n_{z_j}\mathbf{e}_\mathbf{z}(s_j) \tag{4}$$

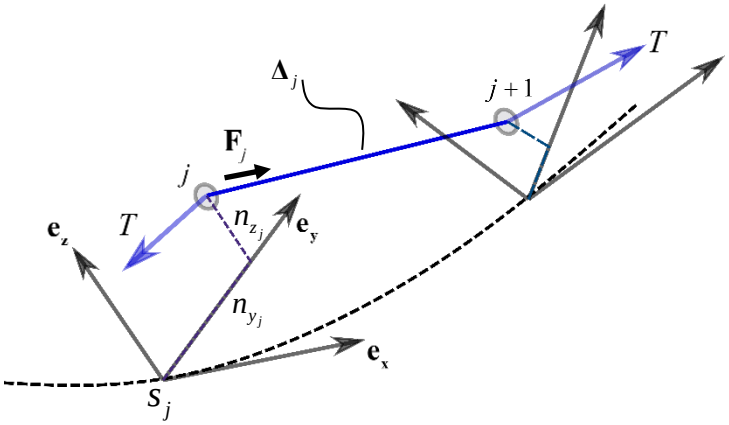

Figure 2: Geometry between the tendon guides and force orientations

The *j*th tendon segment slides between the *j*th and the (*j*+1)th guides and is placed along the vector $\boldsymbol{\Delta}_j = \mathbf{r}_{j+1} - \mathbf{r}_j$.

With the massless assumption eliminating the need to model additional transversal movements of the tendon, its *j*th segment will always be given by $\boldsymbol{\Delta}_j$ during motion. Moreover, with the assumed constant tension, it will be a function of the totality of the Euclidean lengths of the segments:

$$T(\mathbf{q}) = k\left(\sum_j \|\boldsymbol{\Delta}_j\| - l_o\right) + c\overbrace{\frac{d}{dt}\left(\sum_j \|\boldsymbol{\Delta}_j\|\right)}^{=\sum_j\left(\frac{\boldsymbol{\Delta}_j^{\mathrm{T}}\dot{\boldsymbol{\Delta}}_j}{\|\boldsymbol{\Delta}_j\|}\right)} \tag{5}$$

where *k* is its axial stiffness, *c* is the axial viscous damping coefficient and l_o is the initial (unstrained) length of the tendon. A pair of tensile forces corresponding to a segment *j*, placed between the guides *j* and *j*+1, is given by $\mathbf{F}_j$ and $-\mathbf{F}_j$, where:

$$\mathbf{F}_j = T\frac{\boldsymbol{\Delta}_j}{\|\boldsymbol{\Delta}_j\|} \tag{6}$$

Noting that the work imparted by the tension directed along the segment *j* under infinitesimal displacements of the guides *j* and *j*+1 is given by $\mathbf{F}_j^{\mathrm{T}}(\delta\mathbf{r}_j - \delta\mathbf{r}_{j+1}) = -\mathbf{F}_j^{\mathrm{T}}\delta\boldsymbol{\Delta}_j$, while the totality of the work done across all the guides can be compiled:

$$\delta\mathbf{q}^{\mathrm{T}}\mathbf{Q} = -\sum_j \left(\frac{T}{\|\boldsymbol{\Delta}_j\|} \boldsymbol{\Delta}_j^{\mathrm{T}} \delta\boldsymbol{\Delta}_j \right) \tag{7}$$

On substituting (5), the expression can be written in terms of the stiffness, damping and the initial length:

$$\delta\mathbf{q}^{\mathrm{T}}\mathbf{Q} = -\sum_j \left[\left(\frac{k}{\|\boldsymbol{\Delta}_j\|} \left(\sum_f \|\boldsymbol{\Delta}_f\| - l_o \right) + \frac{c}{\|\boldsymbol{\Delta}_j\|} \sum_f \left(\frac{\boldsymbol{\Delta}_f^{\mathrm{T}} \dot{\boldsymbol{\Delta}}_f}{\|\boldsymbol{\Delta}_f\|} \right) \right) \boldsymbol{\Delta}_j^{\mathrm{T}} \delta\boldsymbol{\Delta}_j \right] \tag{8}$$

The individual contributions to each equation *i* in the system (3) can be identified by the corresponding variational term resulting from δq_i.

2.3 Computational methods

In order to extract modal characteristics with the help of the nonlinear model, modal analysis is carried out using linearisation about the calculated nonlinear equilibrium configurations. The method employed is identical to the approach used in 0 where this was implemented to predict static and dynamic instabilities induced by a pre-stressed tendon about the changing deformed static equilibria.

The procedure covering the computation of (nonlinear) static equilibria, linearisation and modal analysis can be summarised through the following sequence:

- Static equilibrium solutions $\hat{\mathbf{q}}_m$ were computed using (7), directly against a set of values of $\{T_m\}$, ($m = 1, 2, \ldots$). This was achieved using the *fsolve* functionality of MATLAB's optimisation toolbox.
- The finite stiffness was included following this: Given a set of tendon stiffness of interest: $\{k_n\}$, ($n = 1, 2, \ldots$), the unstrained lengths $\{l_{o_{m,n}}\}$ corresponding to each T, k combination can be computed using (5) with $\dot{\mathbf{q}} = \mathbf{0}$, such that the static solution $\hat{\mathbf{q}}_m$ corresponds to this combination.
- A numerical linearisation is performed about $\hat{\mathbf{q}}_m$, this time with the tendon's influence included via (8), using the parameters $l_{o_{m,n}}$ and k_n. At this point, any level of damping *c* can be included as this does not affect the correct equilibrium solution $\hat{\mathbf{q}}_m$. The resulting linear eigenvalue problem is solved to extract the modal properties corresponding to T_m - k_n (and *c*) combination.

This solution procedure is adopted due to the simplified process that allows a single equilibria computation to be translated towards the study within a range of axial stiffnesses. In terms of presenting the final results, the equilibrium tension *T* is used (along with *k* and *c*).

3 Experimental study

Experimental work was conducted to support initial exploration of the trends predicted by the model. The primary focus of this study was to establish the trends between the applied tendon loading measure and the identified natural frequencies. The choice of the highly flexible beam was driven by this reasoning, as it exhibits a geometrically nonlinear characteristics – including under its own self-weight induced deformation where the coupling between torsion and in-plane bending was previously observed.

3.1 Test setup

The investigated configuration consisted of a 44.3 cm long steel ruler (beam) with a 1 mm×30 mm rectangular cross-section equipped with three elements used to guide a fine fishing line (tendon) which was passed between the tip and root of the beam, as shown in Figure 3. The tendon comprised of a nylon monofilament line with a 0.35 mm diameter and a total unstrained length of 86 cm. The light, axially soft tendon was chosen to suppress the presence of the tendon-driven modal activity with its reduced modal mass and to highlight the influence of the applied tension/deformation over its axial stiffness during initial experimentation.

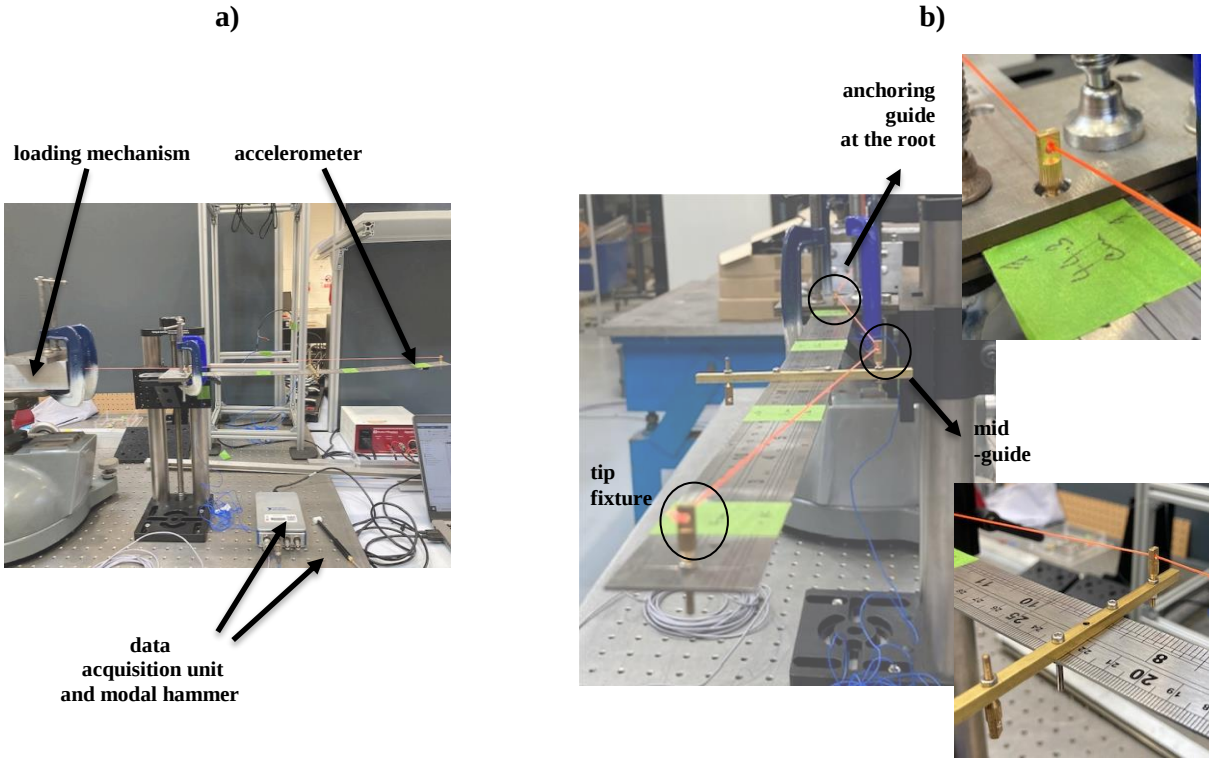

Figure 3: Experimental configuration. (a) Equipment set-up, (b) Geometrical arrangement of the guides

The root anchoring guide and the tip fixture placed 5 mm from the ruler's tip, were situated approximately 1 cm above the centre line of the beam. The mid-span guide was situated eccentrically at a 3.5 cm offset from the central axis of the ruler with a vertical offset of 1.35 cm. The guides, made of small brass eyebolts, had their openings chamfered to allow for smooth axial motion of the tendon.

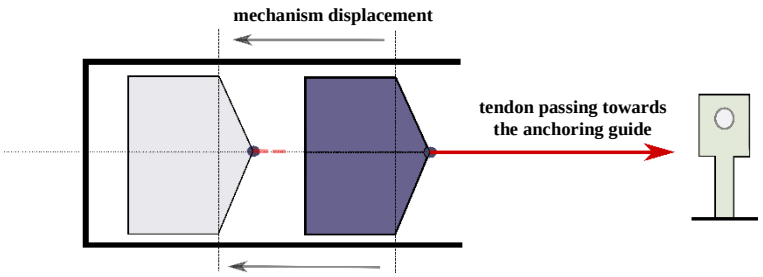

Figure 4: Illustration of the displacement control and loading mechanism

The end of the cable was linked to a loading mechanism that allowed the cable to be pulled along a guided track (Figure 4). The distance along the track was recorded as an indicator of the controlled parameter. From a modelling perspective, neglecting the occurrence of plastic deformation and stiffening, this corresponds to a situation where the stiffness k is held constant, and the mechanism's controlled displacement determines the applied load T at the static equilibrium. The mechanism's displacement is linked to the unstrained length obtained from (5), specifically at a fixed offset from this value to account for the fixed length between the mechanism and the anchoring guide, and any residual loading induced at the 'zero position' of the mechanism.

The collocated Frequency Response Functions (FRFs) were collected experimentally for each deformed equilibrium configuration using an impact hammer and a light single-axis accelerometer attached at the tip of the beam. These were recorded along with the corresponding displacement in the loading mechanism.

3.2 Experimental observations

Figure 5 compares the identified and predicted natural frequency trends. The presented graphs illustrate the variations of the modal frequencies as a function of the distance travelled along the track of the loading mechanism.

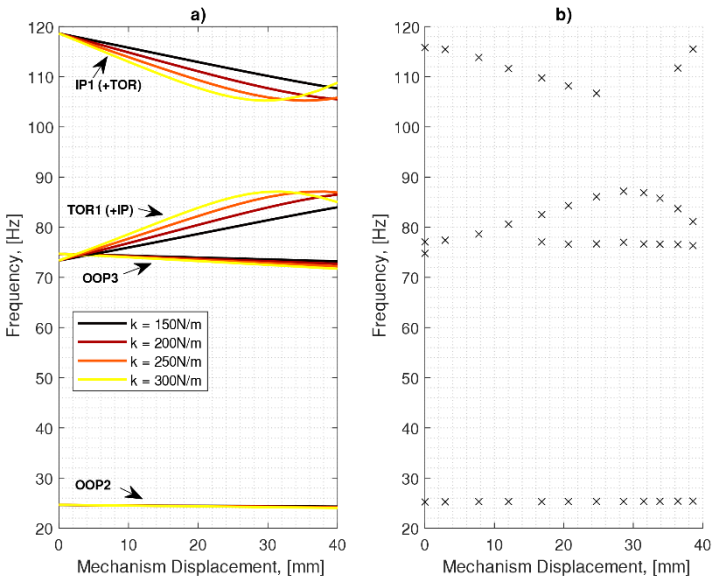

Figure 5: Natural frequency changes due to tendon displacement loading: (a) model predictions for a range of the tendon stiffnesses, (b) experimental results during the loading increments

With the studied experimental case, it was observed that the displacement-based loading induced significant changes on the coupled in-plane (IP) and torsional modes (TOR), with the torsion-dominated mode (TOR1) being increasingly stiffened as the tension is raised. This trend is in line with the model prediction which follow a comparable trend. This further highlights the significance of the nonlinear capability in the implemented model, as the frequency shifts are experienced partly as a result of the topological changes about the nonlinear equilibrium about which the system is systematically linearised.

However, the exact rate of change of the torsional (TOR1) and the in-plane bending (IP1) frequencies could not be matched along with the mechanism's displacement at their veering region. This is assumed to be partly the case due to the axial stiffening that occurred during the loading process. These experimental results are presented against the measured displacement-loading input which offers insufficient information about the actual applied loads. In case of plastic deformation and axial stiffening of the cable, the displacement measurements do not correctly account for the associated increments in loads and the overall

tendon length. Moreover, other unmodelled physical behaviour, such as friction, could influence the discrepancies between the modelled and observed trends.

4 Numerical study

4.1 Dynamics of nominal structure

This numerical study investigates the dynamics of a slender beam that is representative of a high aspect ratio wing. The inertia and stiffness parameters are selected such that the structure is susceptible to bending-torsion coupling under external loading. Accordingly, the parameters are derived based on 0 with some adjustments made to simplify the model and to induce the intended coupling.

Table 1: Beam mechanical properties

Parameter	Value	Parameter	Value
Length, L	0.45 m	Mass per unit length, m	0.25 kg/m
OOP bending rigidity, EI_1	0.5 Nm^2	Torsional inertia, m_{xx}	2.5E-4 kgm
IP bending rigidity, EI_2	16 Nm^2	OOP rotation inertia, m_{yy}	~0
Coupled bending rigidity, EI_{12}	0	IP rotation inertia, m_{zz}	2.5E-4 kgm
Torsional rigidity, GJ	0.75 Nm^2	EA-mass centroid offset, e	0

Figure 6 summarises resulting modal characteristics of the nominal structure:

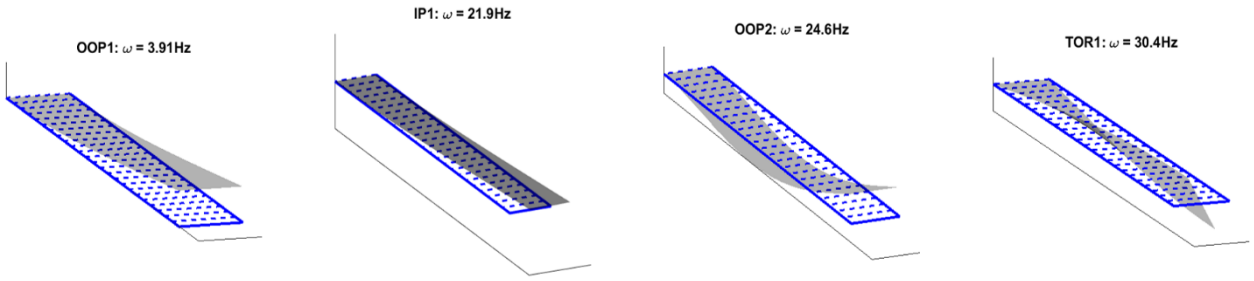

Figure 6: Mode shapes of the nominal structure

It can be seen that the resulting modal frequencies are consistent with those observed in 0. Particularly, the second out of plane bending mode (OOP2) is placed just below the first torsional mode (TOR1).

4.2 Dynamics of augmented system

To support this initial exploratory study, an arbitrary configuration is used where the tendon is guided using three span-wise points. One point is placed at the root (anchor guide), second point at the mid-span position and third point is located at the tip. All guides are offset from the elastic axis. The chord-wise (in-plane) offsets are alternated between the adjacent guides and the guide at the mid-length position includes a significant horizontal offset. The geometrical details of their placements are summarised in Table 2.

Table 2: Geometrical details of the positions of the guiding elements

	s	n_y	n_z
I	0	-5.0% L	3.3% L
II	50% L	5.0% L	3.3% L
III	100% L	-5.0% L	3.3% L

Initially, the effect of the applied tension is demonstrated. Figure 7 illustrates the lengthwise variation of the twist and transversal deformations with the applied axial loading. Figure 8 demonstrates the deformed static geometry under a single loading case. Note that, as discussed previously, the deformation can be computed solely as a function of the applied load. As illustrated, due to the asymmetric placement of the mid-span guiding element, the deformations consist of the coupled transversal and torsional displacements.

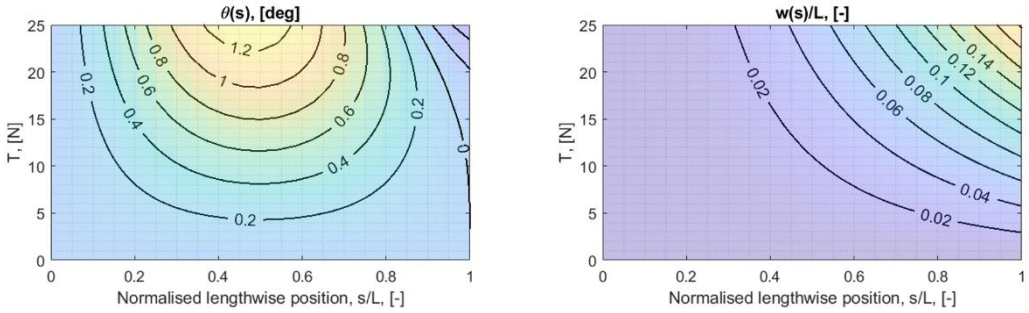

Figure 7: Variations of the lengthwise distribution of the transversal displacements and twist angles at the static equilibria corresponding to varying levels of tension

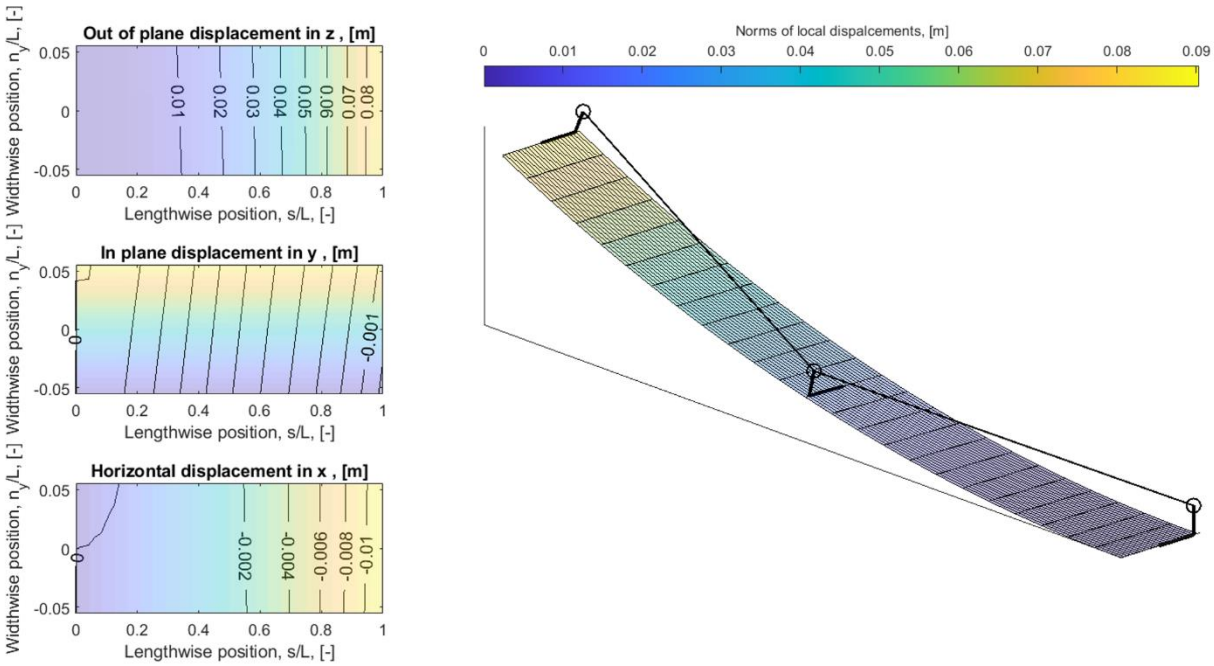

Figure 8: Computed static equilibrium deformation at T = 25 N

Following this, the effect of the axial tendon stiffness can be included. This is achieved by computing the total length of the tendon at the investigated static equilibria, i.e., for each tension, following which the corresponding unstrained length l_o is determined for each level of stiffness. The full equations of motion

are then developed using the parameters k, l_o, which are then linearised numerically about the calculated equilibrium configuration to perform modal analysis (as detailed in section 2.3).

Figure 9 below shows the variations of the modal characteristics for increasing levels of the applied tension at the selected values of stiffnesses.

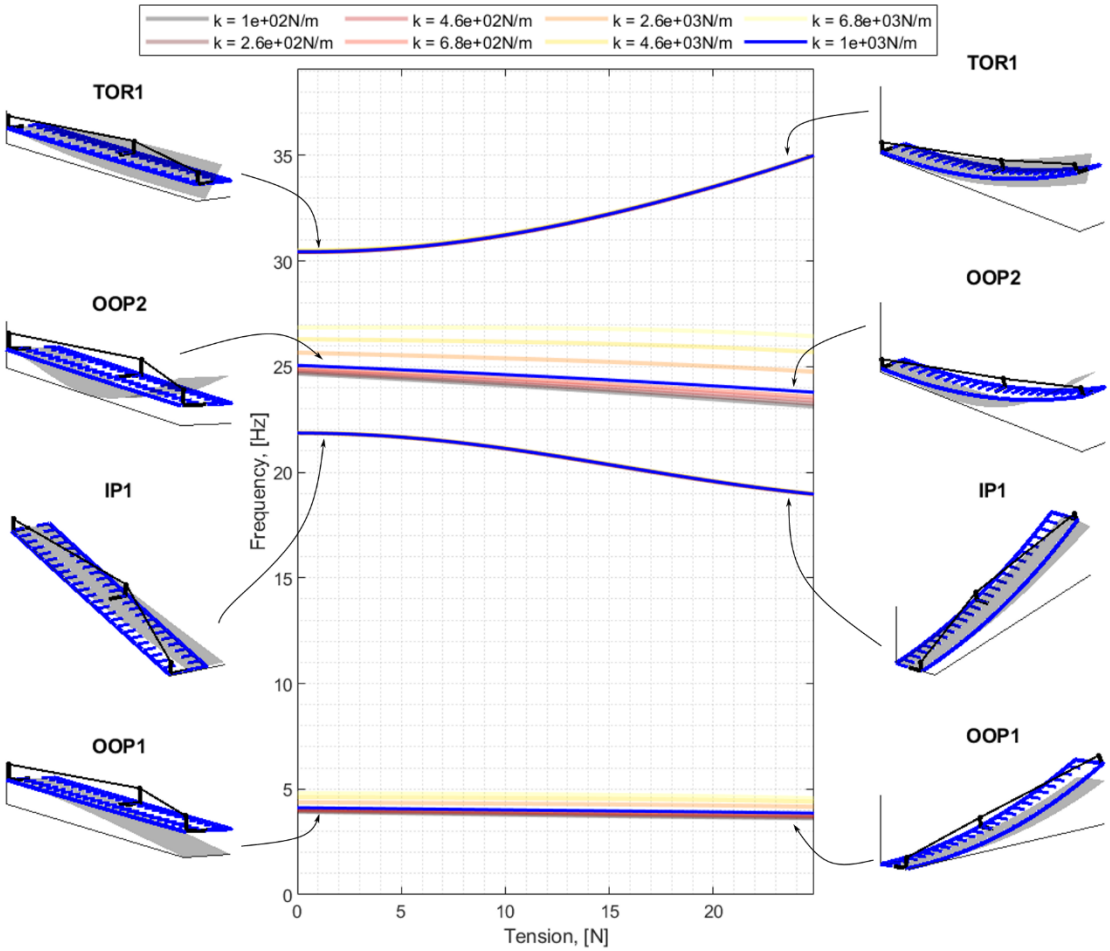

Figure 9: Effect of increasing pre-tension at k = 1000 N/m (with selected other levels of stiffness superposed for comparison)

As illustrated, given the considered geometry of the studied problem, the application of axial loading has opposing effects on the bending and torsional modes. The natural frequencies corresponding to the bending modes are generally subjected to a slight reduction under moderate tensile loading. The softening mechanism leading to this can be related to compressive load induced on the beam, as the structure approaches a static instability referred to as buckling. This factor was also studied in previous beam-tendon studies 0, where it was noted that the critical ('buckling') load can be increased on introducing increasing numbers of intermediate guides.

On the other hand, the torsional frequencies are subjected to an increment. This stiffening phenomenon can be related to the influence of the torsional activity on the projections of the loads between adjacent guides. More specifically, given the eccentric placement of the guides relative to each other, relative torsional activity between adjacent guides results in increased restoring moments due to the altered projections of the tendon's axial load on the guides.

In addition to the effect of tension, Figure 9 also represents the influence of varying the axial stiffness of the tendon. The greatest sensitivity to variations of stiffness is observed on the out of plane bending modes (OOP modes) all of which are subjected to stiffening. The sensitivity of a specific mode to axial stiffness can be indicative of the level of cumulative extensional activity of the tendon within the mode. In the present

case, the greatest level of sensitivity is observed on the second bending mode (OOP2), which is rapidly stiffened under increasing levels of *k*.

However, the torsional and the in-plane bending modes are not strongly influenced by the axial stiffness. This suggests that these modes do not trigger a sufficient extent of axial activity of the tendon given the studied placement of the guides.

To this end, three mechanisms by which the introduced tendon influences the structure was discussed: Namely, the compressive influence on the structure, the influence from the geometrical projections between guides and the extensional activity of the tendon that reflects the axial properties of the tendon. These characteristics can be exploited to introduce favourable dynamical qualities in slender wings, particularly by influencing bending-torsional modal interactions to supress associated instabilities (e.g., see reference 0).

The above results focused on the undamped scenario where only the axial stiffness of the tendon was considered. Developing this study further, Figure 10 illustrates the effects induced by the introduction of the axial tendon damping at the selected value of the axial stiffness, k = 1000 N/m. As shown, the introduction of axial damping has twofold effect on the modal damping values and the natural frequencies.

The influence of axial damping on modal frequencies is comparable to the observations made with increasing axial stiffness, particularly with the increasing out of plane (OOP) bending frequencies being the most influenced. As with the stiffness, this is a result of the varying levels of the tendon's extensional activity between individual modes. Moreover, increasing the axial damping generally causes the modal frequencies to asymptotically approach a 'locked' frequency. The modal damping values, however, initially increase towards their maxima, following which they drop toward the zero values, as the frequencies approach their 'locked' state, implying the reduced dissipation activity. Based on this, for the modal damping values to be maximised, an optimum level of axial damping needs to be identified. This behaviour can be related to the innate link between the dissipative capacity and the level of axial activity of the tendon, which is increasingly suppressed when exceeding the optimum values of axial damping. It is worth mentioning that the identified trends are directly comparable to those observed in 0.

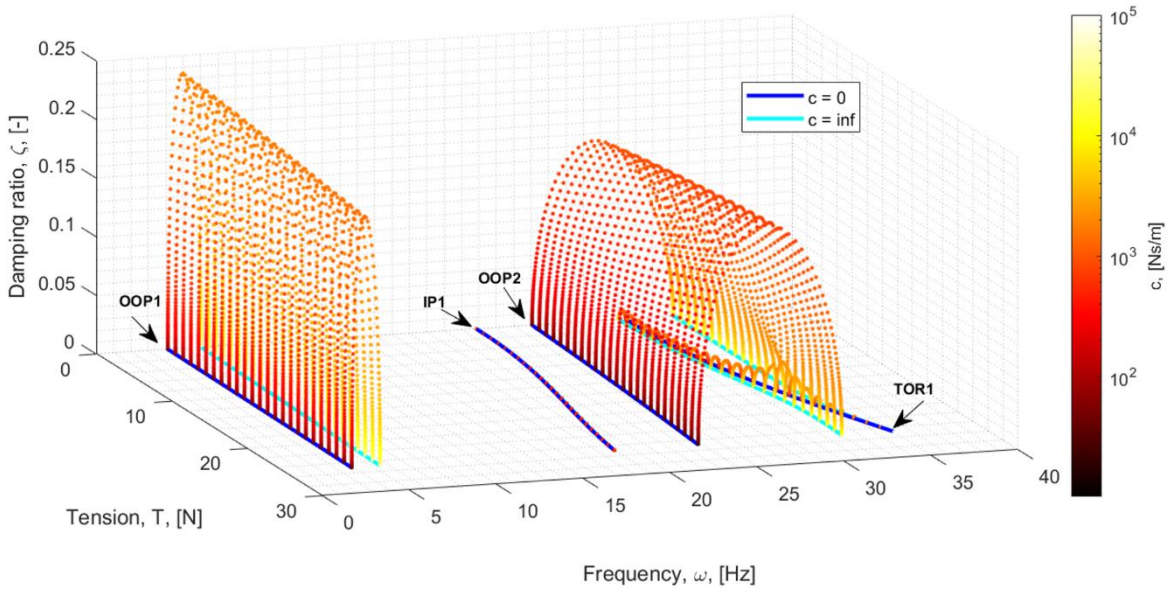

Figure 10: Effect of introducing axial damping at k = 1000 N/m

Another noticeable characteristic is the influence of tension on the level of damping within the torsional mode and the separation between the corresponding locked frequency and the initial undamped frequency. This highlights the combined effect of the extensional activity related and the internal load projection/geometry related influencing mechanisms on this mode.

5 Conclusions

A slender beam with an axially viscoelastic tendon passed across a series of eccentrically placed guides was studied. Numerical analysis, consisting of linear modal analysis about the nonlinear static equilibria, was performed using a nonlinear structural model developed using the Rayleigh-Ritz method, with an experimental test case to confirm the observed trends. Significant modal interactions arising from geometric nonlinearities induced by the deformations caused by the loaded tendons were correlated and confirmed against the experiment.

Following the numerical studies, the following key observations were made surrounding the tendon's axial stiffness, damping and the applied tension:

- The applied tension can have a significant influence on the equilibrium states, particularly with the inclusion of eccentrically placed guides where bending-torsion coupled deformations are observed. The modal characteristics can also be altered using the tension with the level of sensitivity observed being mode-specific: Bending modes generally are softened due to the compression of the structure and the torsional modes are stiffened, particularly with the presence of eccentrically placed guides.
- The influence of the axial stiffness was noted to be mode-specific, being highly dependent on the level of tendon extension related to the modal activity. In the studied scenario, the out of plane bending modes were found to be the most sensitive to changes of axial stiffness.
- Introducing axial damping had the general effect of increasing the modal frequencies as they asymptotically approached fixed ('locked') values. In the context of improving the achievable levels of modal damping, it was observed that an optimum value of the tendon axial damping coefficient can be identified.

Overall, the potential use of a guided tendon as a mean of tuning the modal characteristics of a slender structure was demonstrated. Future work surrounding this concept must cover detailed experimental investigations to interpret the influence of the viscoelastic properties and the limitations arising from the present modelling approach. With further development, the studied architecture could potentially be exploited as a host system that allows inclusion of other wing control mechanisms.

References

[1] F. Afonso, J. Vale, *et al*, "A review on non-linear aeroelasticity of high aspect-ratio wings". *Progress in Aerospace Sciences*, vol. 89, pp. 40-57, 2017

[2] D. Tang, E.H. Dowell, "Experimental and Theoretical Study on Aeroelastic Response of High-Aspect-Ratio Wings". *AIAA Journal*, vol. 39, no. 8, 2011

[3] J. Zhou, M. Xu, *et al*, "Passive Suppression of Panel Flutter Using a Nonlinear Energy Sink". *International Journal of Aerospace Engineering*.

[4] A.G. Cunha-Filno, A.M.G de Lima, *et al*. " Flutter suppression of plates using passive constrained viscoelastic layers". *Mechanical Systems and Signal Processing*. vol. 79, pp. 99-111, 2016.

[5] J. Rocha, P. Moniz, *et al*. "Aeroelastic Control of a Wing with Active Skins Using Piezoelectric Patches". *Mechanics of Advanced Materials and Structures*. vol. 14, pp. 23-32, 2007.

[6] F. Hernández, R. Astroza, *et al*. "A experimental study of a cable-pulleys spring-damper energy dissipation system for buildings". *Journal of Building Engineering*. vol. 51, 2022

[7] A. Sabino, A. Mannella, et al. "Seismic Response of a Structure Equipped with an External Viscous Damping System". *Journ. of Buildings*. vol. 10. 2020.

[8] V. Ondra, B. Titurus. "Free vibration and stability analysis of a cantilever beam axially loaded by an intermittently attached tendon". *Mechanical systems and Signal Processing*. vol. 158, 2021.

[9] J. Wu. B. Titurus. "Vibration control of a rotating Timoshenko beam-tendon system via internal guiding inerter-dampers". *Journ. of Sound and Vibration*. vol. 516, 2022.

[10] S. Jayatilake, M. Lowenberg, B. Woods, B. Titurus. "Aeroelastic and gust rejection characteristics of a slender wing suspended by a viscoelastic cord". in *Proceedings of the International Forum for Aeroelasticity and Structural Dynamics*. Madrid 2022

[11] S. Jayatilake, B. Titurus. "Nonlinear aeroelastic analysis of a damped elastica-aerofoil system". *Nonlinear Dynamics*. May 2022.

[12] D.H. Hodges, E.H. Dowell, "Nonlinear equations of motion for the elastic bending and torsion of twisted nonuniform rotor blades", *Tech. rep., NASA*, Technical Note, 1974.